A new intermediate polymorph of 1-fluoro-adamantane and its second-order like transition towards the low temperature phase

*Lina Yuan,[a] Simon Clevers,[a] Antoine Burel,[a] Philippe Negrier,[b] Maria del Barrio,[c] Bacem Ben Hassine,[b,c] Denise Mondieig,[b] Valérie Dupray,[a] Josep Ll. Tamarit [c] and Gérard Coquerel [a]**

[a] Normandie Université, Laboratoire SMS-EA3233, Université de Rouen, F-76821, Mont Saint Aignan, France.

[b] LOMA, UMR 5798, CNRS, Université de Bordeaux, F-33400 Talence, France.

[c] Grup de Caracterització de Materials, Department de Física, EEBE, Campus Diagonal-Besòs, Eduard Maristany, 10-14, Universitat Politècnica de Catalunya, 08019 Barcelona, Catalonia, Spain.

KEYWORDS: 1-fluoro-adamantane, phase transition, polymorph, temperature-resolved second harmonic generation, X-ray powder diffraction.

ABSTRACT

Phase transitions of 1-fluoro-adamantane have been thoroughly investigated by temperature-resolved second harmonic generation (TR-SHG) and X-ray powder diffraction (XRPD). A new polymorph --- an intermediate centrosymmetric phase (MT) --- between the known orientationally disordered high temperature phase (HT, $F\mathrm{m}\bar{3}\mathrm{m}$, Z=4) and low temperature phase (LT, $P\bar{4}2_1\mathrm{c}$, Z=2) was unveiled by TR-SHG. The crystal structure of MT was resolved by XRPD in the $P4_2/\mathrm{nmc}$ (Z=2) space group and it is related to the LT phase in a group-subgroup relation. No evidence of any solid-solid transition between these two phases by differential scanning calorimetry (DSC) or cold-stage microscope could be obtained. Therefore, combing TR-SHG, XRPD, DSC and cold-stage microscope results, a second-order transition mechanism is proposed for MT↔LT transition. Moreover, the critical exponent (β) of order parameter was calculated by fitting TR-SHG data to a critical power law. The obtained β value (0.26) is close to the value from XRPD data (0.25).

INTRODUCTION

Diamondoids formed by carbon cages have received a great interest, in particular, for building up organic crystals with large cavities and specific physical and chemical properties[1–5]. The simplest diamondoid, adamantane and its derivatives exhibit an orientationally disordered (OD) phase (plastic phase) and show rich polymorphic transitions upon temperature or pressure changes[6–11]. 1-Fluoro-adamantane (1-F-A hereafter, Figure 1) is one of the 1-substituted adamantane and, up

to date, two polymorphs have been revealed: one OD phase at high temperature (HT) and a less disordered low temperature phase (LT).

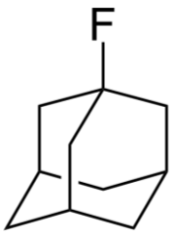

Figure 1. Molecular structure of 1-fluoro-adamantane (1-F-A).

The phase transition HT ↔ LT was first detected by differential scanning calorimetry (DSC) at 222K (upon heating) with an enthalpy of 1.5 kJ/mol.[12] Later, N. T. Kawai et al[13] reported the transition occurs at 227K with an enthalpy of 1.7 kJ/mol upon cooling and at 231K with an enthalpy of 1.6 kJ/mol upon heating. The transition displays a hysteresis which indicates a first-order behavior in the Ehrenfest classification.[14] HT phase has been widely studied by thermal analysis[12], X-ray diffraction[15], NMR[8], single-crystal Raman scattering[16], dielectric analysis[17], and incoherent quasi-elastic neutron scattering[18]. The structure of the HT phase was determined as face-centered cubic ($F\mathrm{m}\bar{3}\mathrm{m}$) by single-crystal X-ray diffraction[15] and by X-ray powder diffraction (XRPD)[19]. However, less was known about the LT phase before the recent publication by Ben Hassine *et. al*[19], in which reported the resolution of the crystal structure of LT phase at 100K by XRPD in the tetragonal non-centrosymmetric $P\bar{4}2_1\mathrm{c}$ space group (Z=2) - CCDC number 1455093[19]. The variation of cell parameters and cell volume of 1-F-A was also monitored by temperature-resolved XRPD from 90K to 360K and a sole discontinuity of the lattice parameters across the HT ↔ LT transition was observed. Based on these results, it was presumed in the work of Ben Hassine *et* al.[19] that only two polymorphs exist and, consequently, that the structure of 1-F-A could be resolved in the $P\bar{4}2_1\mathrm{c}$ space group from 90K until the phase

transition towards the HT phase. As the LT polymorph is still disordered (as assessed by NMR and BDS[8,19]), 1-F-A is a perfect candidate to go deeper into the study of molecular motions in the solid states and across polymorphic transitions.

In this mater, Temperature-Resolved Second Harmonic Generation (TR-SHG) can be used to gather valuable information. SHG (Second Harmonic Generation) refers to an optical process in which an electromagnetic wave gives rise to a new wave at half the initial wavelength while traveling through a non-centrosymmetric material.[20–25] The variation of the second harmonic (SH) signal versus temperature can be obtained by TR-SHG. Vogt[26,27] detailed that the temperature dependence of higher-rank tensors describing SHG are related to variations of long- and short-range order. Moreover, Dougherty and Kurtz[21] mentioned that dynamic disorder possibly couples with local polarization fluctuations and then can induce modification in the SH signal. These make TR-SHG a useful tool to detect phase transitions and polymorphs for systems involving symmetry changes in crystalline structures and molecular motions in non-centrosymmetric crystalline phases. TR-SHG has already been applied to monitor transitions between monotropically or enantiotropically related solid phases[28–31], to track ferroelectric-paraelectric phase transitions[32,33] and order-disorder phase transitions[27,34,35] with as a required condition that at least one non-centrosymmetric crystalline structure is involved[20,21,36–39].

In 1-F-A, the HT phase is centrosymmetric and consequently generates no SH signal. The LT phase resolved in a non-centrosymmetric space group generates a SH signal. Thus, the phase transition between the HT phase and the LT phase can be studied by TR-SHG. Through a careful investigation of phase transitions in 1-F-A (especially at low temperatures) by the synergistic approach of combing TR-SHG and XRPD, not only a new polymorph was ascertained in this work but also the knowledge on the mechanism of ordered-disordered transitions was improved.

EXPERIMENTAL SECTION

Materials. 1-Fluoro-adamantane (CAS registry number: 768-92-3) was purchased from ABCR in Germany (98.3% purity, 1.7% impurity of 1-adamantanol). Crystals used in this work were purified by recrystallization from methanol (HPLC grade), the average crystal size was 200 μm. The purity was checked by GC-MS (higher than 99.9%). See SI-1: (a) the purification procedure of commercial 1-F-A and (b) the purity checking process by GC-MS.

Methods

Temperature-Resolved Second Harmonic Generation (TR-SHG). The non-linear optical method has been introduced in our previous papers[28,34,40–43]. 50 mg powder sample was placed in a computer controlled thermal stage (Linkam THMS-600) The sample was scanned at 1 K/min between 100K and 293K. The number and the duration of the TR-SHG analyses were chosen to ensure the best stability of the laser beam and the best stability of the compound under the laser irradiation. Therefore, the points on the TR-SHG curve were recorded every 2K and each point corresponds to the average value of the SH signal recorded over 3 s (the temperature variation during the recording is 0.05K). For each SH signal versus temperature plot, the SH data were normalized using the maximum SH intensity, which was obtained by fitting the SH curve of the raw values.

The SH intensity generated by a given sample depends on numerous parameters (molecular nature, quality of the long-range order, i.e. the crystallinity, crystal structures, size and orientation of the crystals)[20,21]. Therefore, in order to get reproducible results, we ensured that the laser irradiates the same area of the sample (40 mm^2) all along the experiments. The standard

deviation on SH signal was estimated to c.a. 3%, which is mainly due to energy fluctuations of the laser beams.

Differential Scanning Calorimetry (DSC). Thermal analyses were conducted in a Netzsch 204 F_1 DSC apparatus equipped with liquid nitrogen as the coolant. Both the temperature and the enthalpy changes of the calorimeter were calibrated by using the phase transition of cyclohexane and mercury. Samples with a mass of ca. 8 mg (with a maximum deviation of 0.05 mg) were sealed in a 25 μL aluminum crucible. Thermograms were obtained at a scanning rate of 1 K/min. The atmosphere during the measurements was regulated by a nitrogen flux (40 mL/min). Data treatment was performed with Netzsch-TA Proteus V4.8.4 software.

Cold-Stage Microscope. Samples were loaded into an amorphous quartz crucible and set in a THMS-600 temperature stage setup (Linkam, the same as that used in TR-SHG method). Liquid nitrogen was used as the coolant and the nitrogen flux was regulated via an automatic pump. The setup was coupled with a Nikon Eclipse LV100 microscope and connected to a computer for image captures by a CCD camera.

Note that the temperature accuracy of the Linkam at low temperatures was checked. The melting points of O-xylene (249K) and tetrahydrofuran (165K) in HPLC grade were observed by cold-stage microscope. Different heating/cooling rates were used (0.5 K/min, 1 K/min, 2 K/min, 4 K/min and 5 K/min) and compared with DSC results. The temperature difference between cold-stage microscope and DSC was observed to be lower than 1K.

Curve Fitting. Data were fitted to specific expressions by application of the Levenberg-Marquardt (least-squares method) algorithm using the program Origin 10®.

X-ray Powder Diffraction (XRPD). X-ray powder diffraction data were collected by means of a horizontally mounted INEL cylindrical position-sensitive detector (CPS 120) to pursuit a careful structure determination from the HT to LT phases. The detector constituted by 4096 channels was used in Debye-Scherrer geometry. External calibration using the $Na_2Ca_2Al_2F_{14}$ (NAC) cubic phase mixed with silver behenate was performed by means of cubic spline fittings providing an angular step of 0.029° (2θ) between 4° and 120°. Monochromatic Cu $k_{\alpha 1}$ radiation (λ =1.5406 Å) was selected with an asymmetric focusing incident-beam curved quartz monochromator. The samples were introduced into 0.5 mm-diameter Lindemann capillaries which were rotated perpendicular to the X-ray beam direction in order to decrease as much as possible the effects of preferred orientations. Temperature was controlled with an accuracy of 0.1K by means of a liquid nitrogen 600 series cryostream cooler from Oxford Cryosystems.

RESULTS AND DISCUSSION

Characterization of 1-F-A phase transitions by DSC. A single detectable thermal event was observed by DSC between 120K and 300K for a heating rate of 1K/min (Figure 2). Upon cooling, the onset temperature is 226.0±0.3K with an enthalpy of 1.9±0.1 kJ/mol. Upon heating, a hysteresis is observed, with an onset temperature at 231.0±0.2K and an enthalpy of 1.8±0.1 kJ/mol. This thermal event obviously corresponds to a first-order phase transition. These values are consistent with previously reported values from literature[12,13,19]. Note that the use of a higher heating rate (5K/min) led to a similar result (see SI-2).

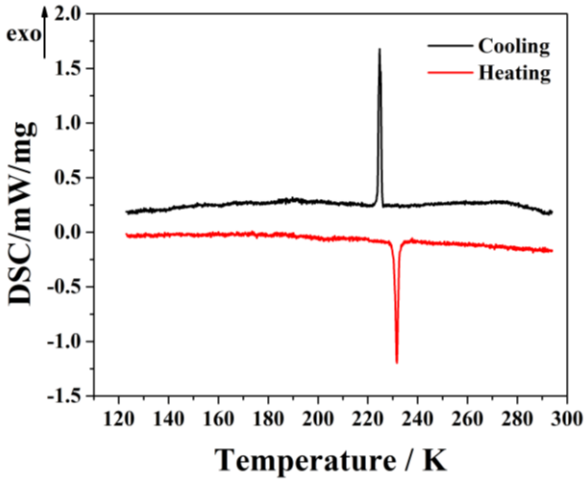

Figure 2. DSC measuring curves obtained for the phase transitions of 1-F-A. Black line, upon cooling (1 K/min); red line, upon heating (1 K/min).

TR-SHG measurements. It is first necessary to mention that in the present case, the intensity of the measured SH signal can be generated only by the non-centrosymmetric crystalline LT phase of 1-F-A. Based on S. K. Kurtz and T. T. Perry[20], SH intensity can be considered proportional to the mass fraction (or molar fraction) of the LT phase.

The thermal evolution of 1-F-A was monitored by TR-SHG through tracking the SH signal generated by the LT phase versus temperature (Figure 3).

Apparently, the sample exhibiting a positive SH signal at 100K, which proves the structure is non-centrosymmetric at this low temperature and confirms the reliability of the XRPD crystal structure determination.[19]

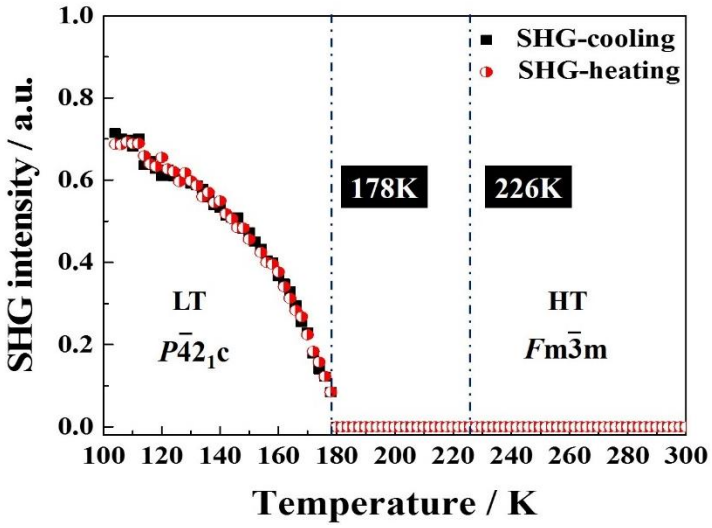

Figure 3. TR-SHG curves obtained for the phase transition of 1-F-A. Black square, upon cooling (1 K/min); red spot, upon heating (1 K/min). The signal appears/disappears at 178K and increases with lowering the temperature down to 100K.

Surprisingly, the SH signal was observed to appear only at 178K (upon cooling) while the transition temperature was detected at 226K by DSC (black curve in Figure 2). The temperature difference is 48K. Obviously, this difference is too large to be caused by the thermal gradient between the sample and the heating plate. Possible reasons for this phenomenon were investigated. Firstly, we supposed that the SH signal generated by 1-F-A between 178K and 226K could have fallen under the detection threshold. Even though the detection threshold of our TR-SHG apparatus can be considered as good (evaluated at circa 1/100 compared to the SH intensity of quartz standard- 45 μm), the sample was annealed at 213K, a temperature between

178K and 226K in order to obtain a better crystallization of the sample (i.e. to possibly enhance the SH signal). After 10 hours, no SH signal was detected (see SI-3), which strongly suggests that no LT phase crystallized in the range of 178K and 226K. Secondly, it was supposed that the transition kinetics might be low and the thermodynamic equilibrium was not reached in this temperature range. So, the sample was annealed at 167K to possibly reach the thermodynamic equilibrium. Nevertheless, after 10 hours, no variation of the SH signal was observed, indicating that the maximum amount of LT phase was already reached under the conditions used for the TR-SHG experiments (see SI-4).

Finally, these results led us to envisage that 1-F-A exhibit an intermediate phase between HT and LT phases in the temperature range of 178K to 226K. In the following, this intermediate phase is referred to as MT (for medium temperature). Since no SH signal was detected between 178K and 226K, MT phase probably exhibits a centrosymmetric crystalline structure (confidence higher than 99%[36]).

Another interesting result is that no hysteresis was observed for the SH signal upon heating and cooling. That is to say, the SH intensity profile is thus completely reversible (*i.e.* thermal cycles after cycles or after stopping and restarting the heating/cooling process). Consequently, a second-order transition between MT ↔ LT can be suspected, complementary with the following observations:

(i) no detectable enthalpy change detected by DSC around 178K;

(ii) no transition front propagation observed by cold-stage microscope (see SI-5);

(iii) no change of the cell volume at the presumed transition temperature (178K) in the work of Ben Hassine et al.[19].

A thorough reinvestigation of the structures resolved from XRPD at various low temperatures confirmed this hypothesis as described in the following.

Crystal structure of MT phase determined from XRPD. When cooling down from HT phase to LT phase, single crystals break and thus powder diffraction is the only way to determine the structure of the low-temperature phases. Therefore, powder X-ray patterns obtained at 90K and 190K were submitted to a Rietveld refinement[44], with the same rigid-body constraints that depicted in the work of Ben Hassine et al.[19]. A single overall isotropic displacement parameter and preferred orientation by using the Rietveld-Toraya function were refined. The final refined patterns together with the experimental and refined pattern differences are shown in Figure 4. The Rietveld refinement converged for LT phase and MT phase to a final R_{wp} value of 6.60% and 6.32%, respectively. The determined crystallographic data of both phases are summarized in Table 1.

A crystal structure validation by Platon[45] was performed on the two resolved space groups. For the LT crystal structure at 90K, Platon results showed that no space group change is needed. While, if the MT phase is resolved in the space group of LT phase (at 190K), missed or additional symmetry are reported and Platon suggested the space group of $P4_2/\mathrm{nmc}$. These results proved that the resolution of the space group in MT and LT phase are robust.

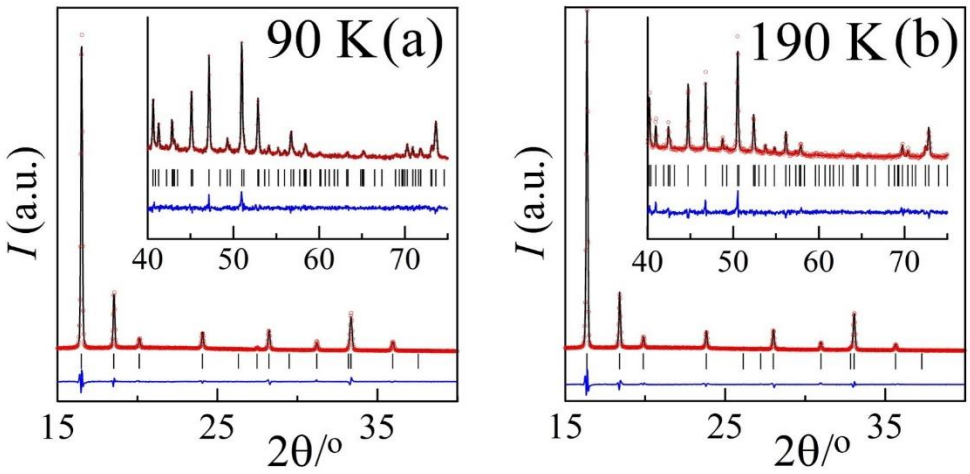

Figure 4. Experimental (red circles) and Rietveld refined (black line) diffraction patterns along with the difference profile (blue line) and Bragg reflections (vertical black sticks) of (a) LT phase at 90K; (b) MT phase at 190K. The insets show the high-angle portion of each pattern (scaled to enhance their visibility).

Table 1. Crystallographic data determined for the MT phase and LT phase.

	MT phase	LT phase
Temperature (K)	190	90
Crystal system	Tetragonal	Tetragonal
Space group	$P4_2/\mathrm{nmc}$	$P\bar{4}2_1\mathrm{c}$
a=b (Å)	6.8145 (5)	6.7696 (4)
c (Å)	8.9232 (9)	8.8211 (9)
Z	2	2
Volume (Å^3)	414.37 (7)	404.25 (6)
Density (g/cm^3)	1.236	1.267

Mechanism of MT ↔ LT phase transition. The presumed second-order phase transition of MT ↔ LT can be confirmed and interpreted microscopically by means of analysis of thermal induced

structural changes. The structure of the LT phase is shown in Figure 5 (a). The angle (ψ) defined between C-F bond of the four equilibrium positions for the statistical-disordered fluorine atoms (i.e., the molecular dipole direction) with the a (or b) tetragonal axis is ca. 6.8^{o} at 90K. Increasing the temperature such angle continuously decreases and at ca. 180K it vanishes and remains null till the phase transition to the HT phase. Such changes provide two new mirror planes perpendicular to the *a* and *b* tetragonal axes. Thus, the non-centrosymmetric space group $P\bar{4}2_1c$ (Z=2) transforms to the centrosymmetric space group $P4_2/nmc$ (Z=2), gives rise to the so-called MT phase, which represents a group-subgroup transition. In addition, lattice parameters as well as volume as a function of temperature do not show any discontinuity (see SI-6). Therefore, the group-subgroup relation, the continuity of the lattice parameters and volume through the LT to the MT phase transition are in agreement with the continuity of the dynamic properties across this second-order phase transition[19].

Figure 5 (b) depicts a structural projection of MT phase along c plane at 190K. It is worth noting that the fractional occupancy of 1/4 of the fluorine atoms remains unchanged across the group-subgroup transition (MT ↔ LT). Therefore, it is probable that the phase transition does not change the type of molecular reorientation and that the dynamics and frequency of molecular motions in the solid state are not (or slightly) modified at the transition temperature (178K). This could be an explanation of why this group-subgroup transition was not highlighted by other techniques such as BDS or solid-state NMR[8,19].

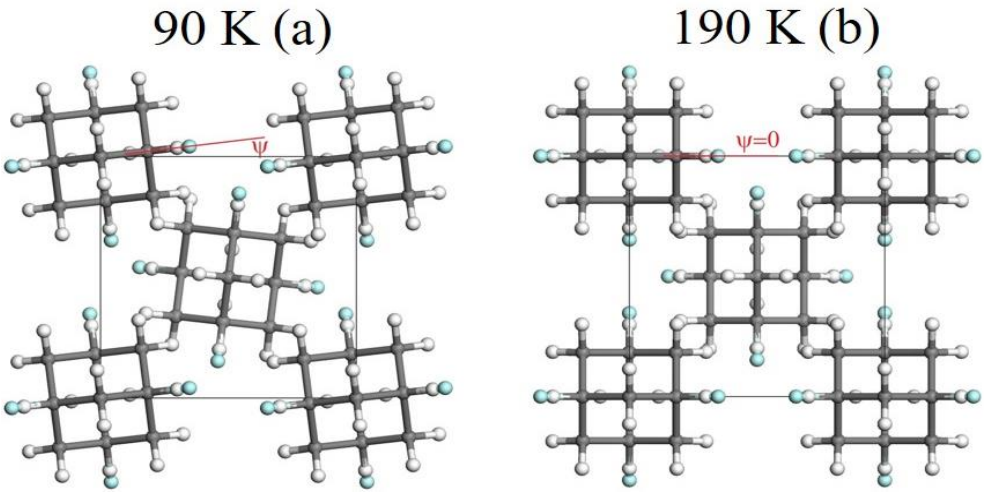

Figure 5. Crystal structure of 1-F-A: (a) LT phase ($P\bar{4}2_1c$, Z=2) at 90K and (b) MT phase ($P4_2/nmc$, Z=2) at 190K. The fractional occupancy of 1/4 of the fluorine atoms (blue) remains unchanged across the MT ↔ LT transition.

To summarize, at 178K, a second-order transition from MT to LT phase starts by a tilt of the angle ψ, as a consequence, an immediate change in the crystal structure. Then this angle ψ increases continuously with decreasing temperature but the crystal structure remains in the LT phase. The above explanations fit well with the TR-SHG results. In Figure 3, the SH signal increases continuously from 178K to 100K. Because SHG is intrinsically related to the crystal structure and molecular fluctuations[36], it suggests that each SH signal corresponds to a LT form in which 1-F-A molecules are tilted at a certain angle (e.g. $\Psi = 6.8^{o}$ at 90K) by thermal agitation.

Variation of the order parameter with temperature. Order parameter η describes the extent of order or disorder in a material. It is equal to unity in the perfectly ordered state and zero in the completely disordered state[46].

TR-SHG was used to track the variation of the order parameter η (according to the Landau theory) versus temperature and to determine the critical exponent β characteristic of this variation.

The temperature dependence of the SH intensity can be expressed as[47]:

$$I_{SHG}(T) \propto (\chi^{(2)}(T))^2 \left[\frac{l^2(T)}{n_1^2(T)n_2(T)} \cdot \frac{\sin^2(\delta(T))}{(\delta(T))^2}\right] \qquad (1)$$

where l is the thickness of the crystals, n_1 and n_2 are the indices of refraction for λ_1=1.064 μm (fundamental beam) and λ_2=0.532 μm (second harmonic beam), respectively. $\chi^{(2)}$ is the non-linear susceptibility tensor, and $\delta = \frac{\pi l}{2l_c}$ with the coherence length $l_c = \frac{\lambda_1}{4|n_1 - n_2|}$.

The term within brackets in equation (1) is generally responsible for a sin-square modulation (sinc^2) of the SH intensity for single crystals. Considering that for powders, the orientations of the crystals are random (averaging over all crystallographic directions) and the particle size (mean value circa 200 μm in the present study) is likely to exceed the coherence length[20], this modulation term can be neglected. Thus, in the following we assume that the SH intensity is proportional to $(\chi^{(2)}(T))^2$. $\chi^{(2)}(T)$ is a third rank tensor with 27 coefficients but the number of independent coefficient can be reduced to 3 in the crystal class $\bar{4}2m$ by symmetry considerations. Moreover, assuming Kleinman conditions[48] are valid (no dispersion and absorption), the number of independent coefficient of the susceptibility tensor can be reduced to only one (d_{14} in the current case) and $\chi^{(2)}(T)$ can be expressed as (in the contracted notation)[49,50]:

$$\chi^{(2)}(T) = 2\begin{bmatrix} 0 & 0 & 0 & d_{14} & 0 & 0 \\ 0 & 0 & 0 & 0 & d_{14} & 0 \\ 0 & 0 & 0 & 0 & 0 & d_{14} \end{bmatrix}$$

Taking into account the previous simplifications, $I_{SHG}(T)$ can be considered proportional to $d_{eff}^2(T)$, where d_{eff} is the effective coefficient of the nonlinear susceptibility. In the present case, d_{eff} is proportional to d_{14} coefficient (using Voigt's convention)[51].

Moreover, d_{14} has already been shown to be a linear function of the order parameter η_{SHG}[35,36] in single crystals. In the present study, measurements are performed on powder samples with random crystallographic orientations but that does not modify the fact that $\chi^{(2)}(T)$ depends only on one coefficient. Therefore, we can assume that the SH signal variations will be the same in all crystallographic directions. Hence, the square root of the SH intensity can be taken as an order parameter:

$$\sqrt{I_{SHG}(T)} \propto d_{eff}(T) \propto \eta \qquad (2)$$

The evolution of the order parameter η with temperature can be described by a simple critical power law derived from Landau theory[35,52]:

$$\eta = A\left(1 - \frac{T}{T_c}\right)^{\beta} \qquad (3)$$

where, A is a pre-factor, T_c is the transition temperature and β is the critical exponent.

Based on the equation (2) and (3), T_c and β values can be extracted from SHG results using:

$$\eta = \sqrt{I_{SHG}(T)} = A\left(1 - \frac{T}{T_c}\right)^{\beta} \qquad (4)$$

The fitting procedure performed from equation (4) with A, T_c and β as free parametersreturns upon cooling a β value of 0.255 ± 0.008 with $T_c = 178.8 \pm 0.3$K. Upon heating, β is 0.263 ± 0.008 with T_c=179.1±0.3K (Figure 6). The experimental transition temperature (T_c: 178K-180K) is thus consistent with the temperature determined by the fitting.

Order parameter η can also be obtained from XRPD by recording ψ (the angle between the molecular dipole C-F bond and the crystallographic a axis) versus temperature (see Figure 6). The XRPD data is fitted according to the power-law (equation (4)), in which A corresponds to $\psi_{(T=0K)}$ and gives rise to $\beta = 0.250 \pm 0.027$ and $T_c = 180.0 \pm 0.1$K. It should be noticed here that the lowest temperature at which the structure was solved was 90K, close to the temperature (92K) at which reorientational motions are characterized by a relaxation time of the order of 100s[19]. Below such temperature, reorientational motions are frozen, according to the previous dynamic study[19] and thus, the LT phase becomes a low-dimensional glass[53–55]. It is obvious that such a LT phase cannot be the stable phase at 0K (the frozen disorder would confer a non-zero entropy) and the true stable phase remains at present elusive. Despite such a thermodynamic evidence, for both TR-SHG and ψ angle data from XRPD, we have assumed a continuous variation with temperature below 90K and renormalization was performed under the hypothesis that order-parameter equals to unity at 0K. Under such assumptions, Figure 6 clearly shows that both TR-SHG and ψ angle from XRPD describe the second-order transition.

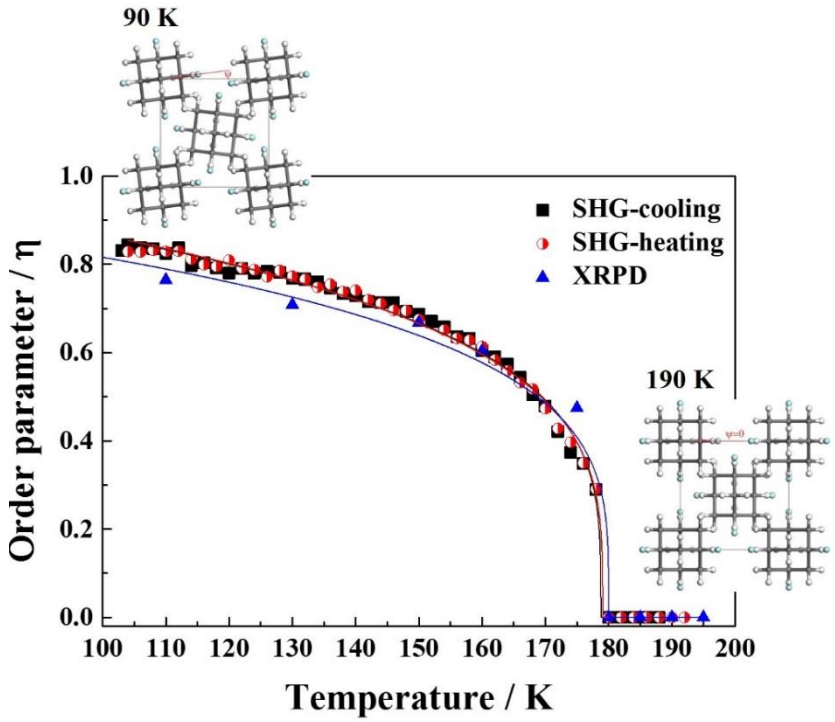

Figure 6. Order parameters determined from normalized values of the TR-SHG data and angle ψ between the C-F bond and a (or b) crystallographic axis from XRPD. Black line corresponds to the fit of equation (4) for the TR-SHG data on cooling (β is 0.255±0.008 with $T_c = 178.8 \pm 0.3$K). Red line corresponds to the fit on heating (β is 0.263±0.008 with $T_c = 179.1 \pm 0.3$K). The blue line corresponds to the fit of XRPD data (β is 0.250±0.027 with $T_c = 180.0 \pm 0.1$K).

CONCLUSIONS

Phase transitions of 1-F-A was thoroughly investigated by using TR-SHG and XRPD. The combination of both techniques unveiled a new phase with a stability domain between 178K and 231K. A second-order transition occurs at 178K between the LT phase ($P\bar{4}2_1c$) and the intermediate temperature phase (MT, $P4_2/\mathrm{nmc}$), which arises from a continuous tilt of the molecules by thermal agitation. A first-order transition occurs at 231K between the MT phase and the high temperature cubic phase HT ($F\mathrm{m}\bar{3}\mathrm{m}$). Moreover, variation of the order parameter

versus temperature for the second-order transition was monitored by TR-SHG and XRPD, results are in good agreement to support the proposed second-order transition mechanism.

In this work, the hint of a second-order phase transition might arouse certain debate as in the literature, for several compounds, second-order transitions finally turned out to be first order transitions[56,57]. For instance, the undetectable thermal signature of theses transitions might be interpreted as inconsistent with thermodynamics. In fact, the structure differences between LT and MT phases are very subtle and the phase transition arises from a slight tilt of the 1-F-A molecule. Neither lattice parameters nor volume show discontinuity at the transition temperature (178K). Consequently, transition between both phases should be difficult even impossible to be detected by usual DSC measurements. Measurement of heat capacity (C_p) at low temperature might give some indications of the MT ↔ LT transition. So, further study of this second-order transition combining other techniques could be suitable. For example, X-ray absorption near edge structure (XANES) might provide certain information about the change of the local symmetry. Finally, this work underlines that the study of polymorphs and phase transitions should be carried out carefully. The combination of TR-SHG and XRPD seems a suitable tool to monitor subtle symmetry changes when non-centrosymmetric structures are involved, such as, in diamondoids. In light of the present study, a thorough reinvestigation of phase transitions in adamantane derivatives could be envisaged.

ASSOCIATED CONTENT

Supporting Information.

Purification procedure for 1-fluoro-adamantane, purity checking process of purified 1-fluoro-adamantane, DSC curve for the phase transitions of 1-F-A measured at 5 K/min heating/cooling rate, TR-SHG curve obtained for 1-fluoro-adamantane by annealing at 213K for 10h, TR-SHG curve obtained for 1-fluoro-adamantane by annealing at 167K for 10h (inset), cold-stage microscopy observations of the phase transition of 1-fluoro-adamantane (video), variations of the unit cell parameter *a*, the unit cell parameter *c* and the volume of 1-fluoro-adamantane in the temperature range of 90K to 220K.

AUTHOR INFORMATION

Corresponding Author

*E-mail: gerard.coquerel@univ-rouen.fr

ACKNOWLEDGMENTS

This work was partially supported by the CICyT (Spain) project FIS2011-24439, and by DGU (Catalonia) project 2014SGR00581.

REFERENCES

(1) McIntosh, G. C.; Yoon, M.; Berber, S.; Tománek, D. *Phys. Rev. B* **2004**, *70* (4), 45401.
(2) Dahl, J. E.; Liu, S. G.; Carlson, R. M. K. *Science* **2003**, *299* (5603), 96–99.
(3) Yang, W. L.; Fabbri, J. D.; Willey, T. M.; Lee, J. R. I.; Dahl, J. E.; Carlson, R. M. K.; Schreiner, P. R.; Fokin, A. A.; Tkachenko, B. A.; Fokina, N. A.; Meevasana, W.; Mannella, N.; Tanaka, K.; Zhou, X. J.; van Buuren, T.; Kelly, M. A.; Hussain, Z.; Melosh, N. A.; Shen, Z.-X. *Science* **2007**, *316* (5830), 1460–1462.
(4) Wang, Y.; Kioupakis, E.; Lu, X.; Wegner, D.; Yamachika, R.; Dahl, J. E.; Carlson, R. M. K.; Louie, S. G.; Crommie, M. F. *Nat. Mater.* **2008**, *7* (1), 38–42.
(5) Guo, W.; Galoppini, E.; Gilardi, R.; Rydja, G. I.; Chen, Y.-H. *Cryst. Growth Des.* **2001**, *1* (3), 231–237.
(6) Affouard, F.; Guinet, Y.; Denicourt, T.; Descamps, M. *J. Phys. Condens. Matter* **2001**, *13* (33), 7237–7248.
(7) Bée, M.; Amoureux, J. P. *Mol. Phys.* **1983**, *48* (1), 63–79.
(8) Decressain, R.; Amoureux, J. P.; Carpentier, L.; Nagy, J. B. *Mol. Phys.* **1991**, *73* (3), 553–569.

(9) Ben Hassine, B.; Negrier, Ph.; Barrio, M.; Mondieig, D.; Massip, S.; Tamarit, J. Ll. *Cryst. Growth Des.* **2015**, *15* (8), 4149–4155.
(10) Negrier, Ph.; Barrio, M.; Romanini, M.; Tamarit, J. Ll.; Mondieig, D.; Krivchikov, A. I.; Kepinski, L.; Jezowski, A.; Szewczyk, D. *Cryst. Growth Des.* **2014**, *14* (5), 2626–2632.
(11) Negrier, Ph.; Barrio, M.; Tamarit, J. Ll.; Mondieig, D. *J. Phys. Chem. B* **2014**, *118* (32), 9595–9603.
(12) Clark, T.; Knox, T. M. O.; Mackle, H.; McKervey, M. A. *J. Chem. Soc. Faraday Trans. 1 Phys. Chem. Condens. Phases* **1977**, *73* (0), 1224.
(13) Kawai, N. T.; Gilson, D. F. R.; Butler, I. S. *Can. J. Chem.* **1991**, *69* (11), 1758–1765.
(14) Jaeger, G. *Arch. Hist. Exact Sci.* **1998**, *53* (1), 51–81.
(15) Amoureux, J. P.; Bee, M.; Sauvajol, J. L. *Acta Crystallogr. Sect. B* **1982**, *38* (7), 1984–1989.
(16) Guinet, Y.; Sauvajol, J. L.; Muller, M. *Mol. Phys.* **1988**, *65* (3), 723–738.
(17) Amoureux, J. P.; Castelain, M.; Bee, M.; Benadda, M. D.; More, M. *Mol. Phys.* **1985**, *55* (1), 241–251.
(18) Bée, M.; Amoureux, J. P. *Mol. Phys.* **1983**, *50* (4), 585–602.
(19) Ben Hassine, B.; Negrier, Ph.; Romanini, M.; Barrio, M.; Macovez, R.; Kallel, A.; Mondieig, D.; Tamarit, J. Ll. *Phys. Chem. Chem. Phys.* **2016**, *18* (16), 10924–10930.
(20) Kurtz, S. K.; Perry, T. T. *J. Appl. Phys.* **1968**, *39* (8), 3798–3813.
(21) Dougherty, J. P.; Kurtz, S. K. *J Appl Cryst* **1976**, *9*, 145–158.
(22) Franken, P. A.; Ward, J. F. *Rev. Mod. Phys.* **1963**, *35* (1), 23–39.
(23) Wanapun, D.; Kestur, U. S.; Kissick, D. J.; Simpson, G. J.; Taylor, L. S. *Anal. Chem.* **2010**, *82* (13), 5425–5432.
(24) Sutherland, R. L. *Handbook of Nonlinear Optics*, 2ed.; Marcel Dekker, Inc.: New York, 2003.
(25) Bloembergen, N. *Nonlinear Optics (World Scientific)*, 4th ed.; World scientific Publishing: Singapore, 1996.
(26) Vogt, H. *Appl. Phys.* **1974**, *5* (2), 85–96.
(27) Vogt, H. *Phys. Status Solidi B* **1973**, *58* (2), 705–714.
(28) Clevers, S.; Simon, F.; Sanselme, M.; Dupray, V.; Coquerel, G. *Cryst. Growth Des.* **2013**, *13* (8), 3697–3704.
(29) Smilowitz, L.; Henson, B. F.; Asay, B. W.; Dickson, P. M. *J. Chem. Phys.* **2002**, *117* (8), 3789–3798.
(30) Smilowitz, L.; Henson, B. F.; Romero, J. J. *J. Phys. Chem. A* **2009**, *113* (35), 9650–9657.
(31) Hall, R. C.; Paul, I. C.; Curtin, D. Y. *J. Am. Chem. Soc.* **1988**, *110* (9), 2848–2854.
(32) Aktsipetrov, O. A.; Misuryaev, T. V.; Murzina, T. V.; Blinov, L. M.; Fridkin, V. M.; Palto, S. P. *Opt. Lett.* **2000**, *25* (6), 411–413.
(33) Bergman, J. G. *J. Am. Chem. Soc.* **1976**, *98* (4), 1054–1055.
(34) Clevers, S.; Rougeot, C.; Simon, F.; Sanselme, M.; Dupray, V.; Coquerel, G. *J. Mol. Struct.* **2014**, *1078*, 61–67.
(35) Steinbrener, S.; Jahn, I. R. *J. Phys. C Solid State Phys.* **1978**, *11* (7), 1337–1349.
(36) Chemla, D. S. *Rep. Prog. Phys.* **1980**, *43* (10), 1191.
(37) Sutherland, R. L. *Handbook of Nonlinear Optic*, 2nd ed.; Marcel Dekker: New York, 2003.
(38) *Appl. Phys. Lett.* **1964**, *5* (1), 17–19.
(39) Donakowski, M. D.; Gautier, R.; Lu, H.; Tran, T. T.; Cantwell, J. R.; Halasyamani, P. S.; Poeppelmeier, K. R. *Inorg. Chem.* **2015**, *54* (3), 765–772.

(40) Yuan, L.; Clevers, S.; Couvrat, N.; Cartigny, Y.; Dupray, V.; Coquerel, G. *Chem. Eng. Technol.* **2016**, *39* (7), 1326–1332.
(41) Clevers, S.; Simon, F.; Dupray, V.; Coquerel, G. *J. Therm. Anal. Calorim.* **2013**, *112* (1), 271–277.
(42) Simon, F.; Clevers, S.; Gbabode, G.; Couvrat, N.; Agasse-Peulon, V.; Sanselme, M.; Dupray, V.; Coquerel, G. *Cryst. Growth Des.* **2015**, *15* (2), 946–960.
(43) Simon, F.; Clevers, S.; Dupray, V.; Coquerel, G. *Chem. Eng. Technol.* **2015**, *38* (6), 971–983.
(44) Rietveld, H. M. *J. Appl. Crystallogr.* **1969**, *2* (2), 65–71.
(45) Spek, A. L. *Acta Crystallogr. D Biol. Crystallogr.* **2009**, *65* (2), 148–155.
(46) Rao, C. N. R.; Rao, K. J. *Phase Transitions in Solids: An Approach to the Study of the Chemistry and Physics of Solids*; McGraw-Hill, 1978.
(47) Boyd, G.; Kasper, H.; McFee, J. *IEEE J. Quantum Electron.* **1971**, *7* (12), 563–573.
(48) Boyd, R. W. In *Nonlinear Optics (Third Edition)*; Academic Press: Burlington, 2008; pp 1–67.
(49) Nye, J. F. *Physical Properties of Crystals: Their Representation by Tensors and Matrices*; Clarendon Press, 1985.
(50) Marder, S. R.; Sohn, J. E.; Stucky, G. D. *Materials for Nonlinear Optics: Chemical Perspectives*; American Chemical Society, 1991.
(51) Dmitriev, V. G.; Gurzadyan, G. G.; Nikogosyan, D. N.; Lotsch, H. K. V. *Handbook of Nonlinear Optical Crystals*; Springer Series in Optical Sciences; Springer Berlin Heidelberg: Berlin, Heidelberg, 1999; Vol. 64.
(52) Bruins, D. E.; Garland, C. W. *J. Chem. Phys.* **1975**, *63* (10), 4139–4142.
(53) Romanini, M.; Barrio, M.; Capaccioli, S.; Macovez, R.; Ruiz-Martin, M. D.; Tamarit, J. Ll. *J. Phys. Chem. C* **2016**, *120* (19), 10614–10621.
(54) Pérez, S. C.; Zuriaga, M.; Serra, P.; Wolfenson, A.; Negrier, Ph.; Tamarit, J. Ll. *J. Chem. Phys.* **2015**, *143* (13), 134502.
(55) Tripathi, P.; Mitsari, E.; Romanini, M.; Serra, P.; Tamarit, J. Ll.; Zuriaga, M.; Macovez, R. *J. Chem. Phys.* **2016**, *144* (16), 164505.
(56) Mnyukh, Y. *Fundamentals of Solid-State Phase Transitions, Ferromagnetism and Ferroelectricity*; AuthorHouse, 2001.
(57) Mnyukh, Y. *ArXiv11021085 Phys.* **2011**.

For Table of Contents Use Only.

Manuscript title: A new intermediate polymorph of 1-fluoro-adamantane and its second-order like transition towards the low temperature phase

Author list: Lina Yuan, Simon Clevers, Antoine Burel, Philippe Negrier, Maria del Barrio, Bacem Ben Hassine, Denise Mondieig, Valérie Dupray, Josep Ll. Tamarit and Gérard Coquerel.

TOC graphic:

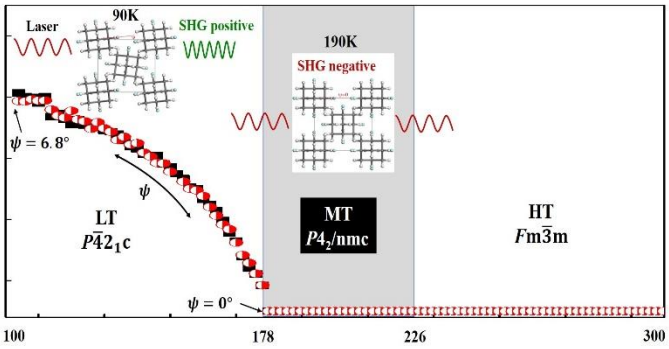

Synopsis: In 1-fluoro-adamantane, a new polymorph (MT) between the known HT and LT phases was unveiled by a combination of TR-SHG, XRPD, DSC and cold-stage microscopy experiments. The crystal structure was resolved in the space group of $P4_2/nmc$. A second-order mechanism is proposed for the MT↔LT transition which arises from a continuous variation of the tilt angle between the molecules.